Journal of Wind Engineering & Industrial Aerodynamics 251 (2024) 105786

Contents lists available at ScienceDirect

Journal of Wind Engineering & Industrial Aerodynamics

journal homepage: www.elsevier.com/locate/jweia

The reproduction of 2-D non-synoptic wind field in an actively controlled wind tunnel

Lin Zhao [a,b,c,d], Liutian Zhang [c], Wei Cui [c,d,*], Shuyang Cao [c,d], Yaojun Ge [c,d]

[a] College of Civil Engineering and Architecture, Guangxi University, Nanning 530004, China
[b] Key Laboratory of Disaster Prevention and Structural Safety of China Ministry of Education, Guangxi University, Nanning 530004, China
[c] State Key Lab of Disaster Reduction in Civil Engineering, Tongji University, Shanghai 200092, China
[d] Key Laboratory of Transport Industry of Wind Resistant Technology for Bridge Structures, Tongji University, Shanghai 200092, China

ARTICLE INFO

Keywords:
Actively controlled wind tunnel
Non-synoptic wind simulation
Typhoon wind spectrum
Non-stationary wind speed

ABSTRACT

This work mainly discusses the simulation of 2-D non-synoptic wind field in a novel actively controlled wind tunnel. The vibrating fins with airfoil shape are installed at the downstream of multiple fans in the updated active wind tunnel, which will work with fans simultaneously to generate 2-D non-synoptic flow. The fins mainly control the vertical flow while the fans control the along-wind flow, and the input signal of equipment can be adjusted in a predefined way. Then, based on Banach fixed-point theorem, the input signal of fans and fins is constantly updated by an iteration-based method to derive the generated wind characteristics to approach the different target values within an acceptable error range. According to the degree of interference between the longitudinal and the vertical wind characteristics, different iteration strategies are proposed for different wind fields. Two typical non-synoptic wind fields are taken as application examples: irregular turbulence spectra in typhoons and non-stationary winds in mountainous terrains. After iterations, both case studies were generated appropriately in the active tunnel. The simulated wind fields are crucial for wind-resistant design of wind-sensitive structures under non-synoptic wind climates.

1. Introduction

Wind tunnel experiments play an important role in the field of industrial aerodynamics. The first step of wind tunnel test is always reproducing the target wind field accurately in wind tunnel, and the main methodologies could be classified into passive simulation (Counihan, 1969, 1973), active simulation (Cao et al., 2001, 2002) and active-passive hybrid simulation (Li et al., 2023). In the 1960s and 1970s, the passive method was first proposed by Counihan to simulated the averaged wind profile and turbulence profile of atmospheric boundary layer (ABL) by spires and rough elements (Counihan, 1969, 1973). Subsequently, the empirical formula of gradient wind elevation simulated by the combination of spires and rough blocks was recommended by Irwin in 1981 (Irwin, 1981). Currently, the passive method has become the most commonly used tool to simulate natural wind climate. However, the wind tunnel flow field in passive simulation is mainly concerned with the wind speed profile and turbulence profile in a synoptic climate. The fluctuating wind power spectrum density function (PSD) and the integral scale reflecting the important characteristics of wind fields are rarely simulated in current wind tunnel.

Considering the fact that turbulence characteristics cannot be represented completely in passive simulation, many researchers took active wind tunnel as an alternative device to reproduce ABL. The active simulation technique improves the simulation of PSD and integral scale by injecting mechanical energy of appropriate frequency into the flow field (Kobayashi and Hatanaka, 1992; Kobayashi et al., 1994). There are two main methods for the active simulation technology of ABL. One is to inject random fluctuating energy into the airflow of the wind tunnel by relying on the vibration motion to achieve active control, mainly including vibrating wings, vibrating spires, etc. For example, a vibrating device was installed in the ABL wind tunnel of Colorado State University. Two rows of vibrating grids vibrated randomly in 4–16 s period, and generated the ABL wind field at downstream (Cermak, 1995).

The other is the fan array with varying rotation frequencies, which relies on the adjustablility of fan speed to provide the high frequency energy and stimulate the formation of turbulent vortices (Kobayashi and Hatanaka, 1992; Kobayashi et al., 1994). This technology was firstly developed in Japan, where prototype came from Teunissen's

* Correspondence to: 320 Wind Engineering Building, Tongji University, 1239 Siping Road, Shanghai, 200092, China.
E-mail addresses: zhaolin@tongji.edu.cn (L. Zhao), zlt@tongji.edu.cn (L. Zhang), cuiwei@tongji.edu.cn (W. Cui), shuyang@tongji.edu.cn (S. Cao), yaojunge@tongji.edu.cn (Y. Ge).

https://doi.org/10.1016/j.jweia.2024.105786
Received 20 October 2023; Received in revised form 3 June 2024; Accepted 3 June 2024
Available online 17 June 2024

multi-jet wind tunnel (Cermak and Cochran, 1992). At early stage, Cao et al. (2001) reproduced the ABL in active tunnel by an iteration-based algorithm. More specifically, targeting at von Kármán type turbulence and utilizing the two-dimensional (2-D) actively controlled wind tunnel, they simulated the profiles of statistical turbulent parameters including Reynolds stress, turbulence intensity, integral scale and PSD simultaneously. After that, the velocity histories of random fluctuating flow and intermittent flow were generated in the three-dimensional (3-D) active tunnel (Cao et al., 2002). Both complicated velocity sequence and statistical turbulent parameters can be simulated in active tunnels. However, the existing research mainly focuses on the wind parameters of the synoptic climates, such as the von Kármán spectrum and the wind profile obeying exponential law, while those of the non-synoptic wind climates are rarely involved.

In recent years, researchers have paid more attention to study the aerodynamics and aeroelastic responses of wind-sensitive structures under different kinds of non-synoptic wind environment such as typhoons (Fang et al., 2020), tornadoes (Hou and Sarkar, 2020) and mountain winds (Zhang et al., 2019). Different from the large-scale synoptic wind, there are often non-Gaussian turbulences (Cui et al., 2022), irregular wind spectra (Liu et al., 2022) and non-stationary wind speeds (Lei et al., 2022) in these unconventional wind climates. It is fundamental to simulate the key turbulent parameters in wind tunnels accurately. Recently, based on the active tunnel developed in Tongji University, Cui et al. (2021) has generated unconventional along-wind flows, such as skewed non-Gaussian turbulence and transient short-duration gust. Subsequently, Dong et al. (2022) investigated the aerodynamic forces and wind-induced responses of a long-span rigid-frame bridge in a mountainous area under strong gust in this tunnel. Zhao et al. (2023) revealed the aerodynamic characteristics of streamlined box girders under shear flows with different velocity gradients, turbulence intensities, and integral scales. Unfortunately, this tunnel only equipped with multiple arrays of fans but without actively controlled vibrating fins, which caused much difficulty in simulating crosswind turbulence, so the previous research did not control the vertical characteristics of flow field.

In order to improve the flow field controllability based on the methodology of multi-fan turbulence generated, a device with actively controlled vibrating fins is design to work together with the purpose of strengthening the crosswind effects. In the updated wind tunnel, the fan array and the fin system operate synchronously to allow longitudinal and vertical turbulence to be adjusted in a predefined way. Generally, an iteration-based process is used to approximate the target wind parameters, and the specific iterative approaches for different wind parameters differ in a few ways based on the coupling relationship between the vertical and longitudinal components in the flow field. Two non-synoptic wind environments: 2-D typhoon wind spectra and 2-D non-stationary wind speeds, are selected as the main simulation objects.

2. The wind tunnel with multiple fans and airfoils

2.1. Original actively controlled wind tunnel

Fig. 1 is the original active wind tunnel, which is an open-circuit one with 120 fans of 270 mm in diameter with the arrangement as 12 (vertical) by 10 (horizontal) matrix. Every fan can be driven and controlled synchronously by AC servomotors and the maximum frequency of fans reaches 20 Hz. The time series of fan speed can be written through the self-defined external control file, and the parameters can be assigned to a single fan, a row of fans, a column of fans or all fans. By adjusting the fan speeds to the maximum, the wind velocity in the test section can be up to 24 m/s. The test section is 1.5 m wide and 1.8 m high. As shown in Fig. 2(a), the wind tunnel is assembled by multiple modules in the longitudinal direction, which means the length of the test section and location of testing model can be adjusted accordingly. Another important fact is that modularity provides a fairly convenient installation interface for flow field control devices such as damping nets and actively controlled fins.

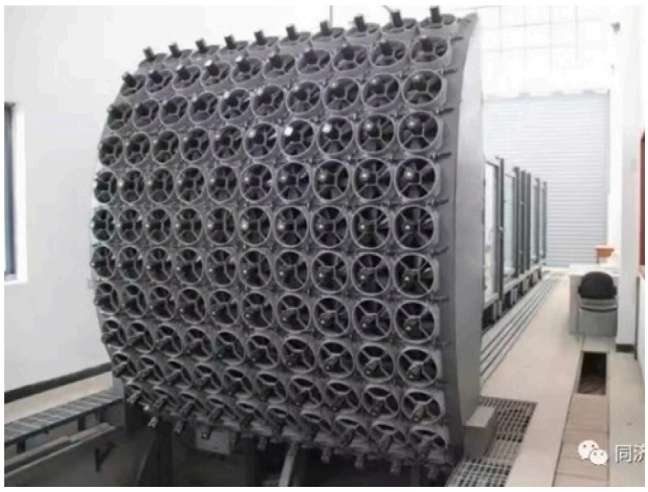

Fig. 1. Fan array of actively multi-fans wind tunnel.

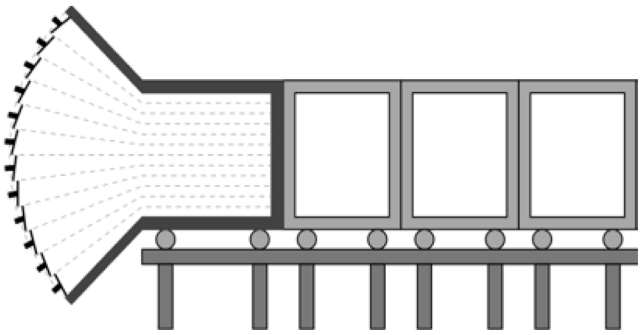

(a) Original active wind tunnel

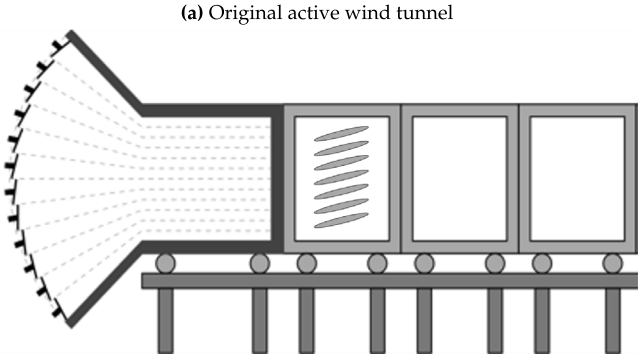

(b) Updated active wind tunnel with fins

Fig. 2. Modularized active wind tunnel.

2.2. Updated actively controlled wind tunnel

In the updated wind tunnel shown in Fig. 2(b), the actively controlled fins is installed after the fan array to improve the simulation performance of the flow field, especially the vertical wind characteristics. Therefore, it is able to actively control the flow characteristics in both the along-wind and vertical directions simultaneously.

The active airfoil system includes a series of airfoils and a mechanical transmission device. As shown in Fig. 3, the main body of the mechanical transmission device is composed of 11 AC servomotors and corresponding supporting rods. The supporting rods connect the motors and the airfoils. Similar to the fan array, the input voltage can be adjusted to the AC servomotor and to drive the corresponding airfoil individually at desired time-variant frequency. Besides, the airfoils and

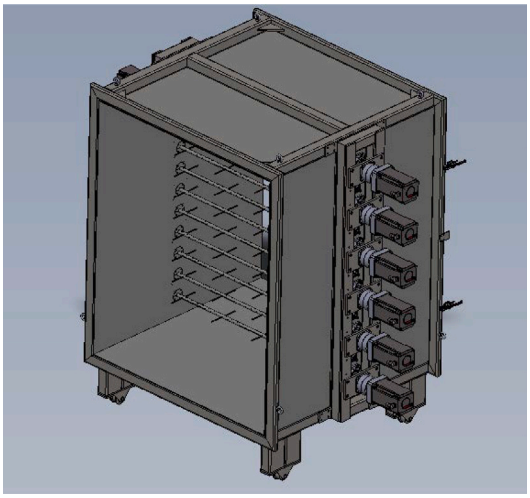

(a) 3D view

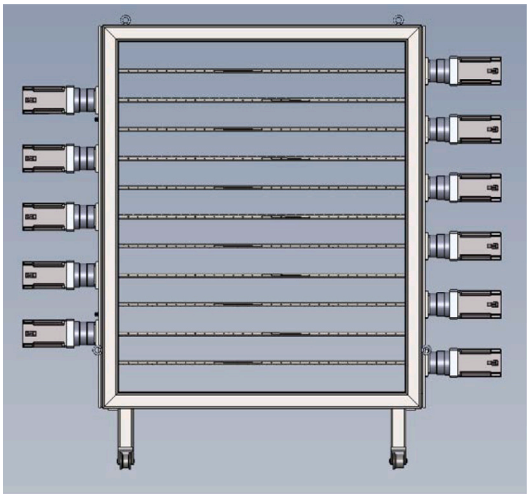

(b) Front view

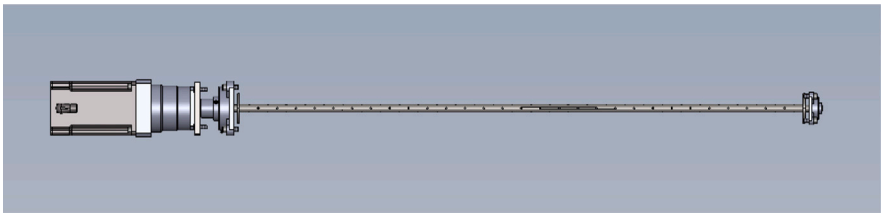

(c) Support rod and motor

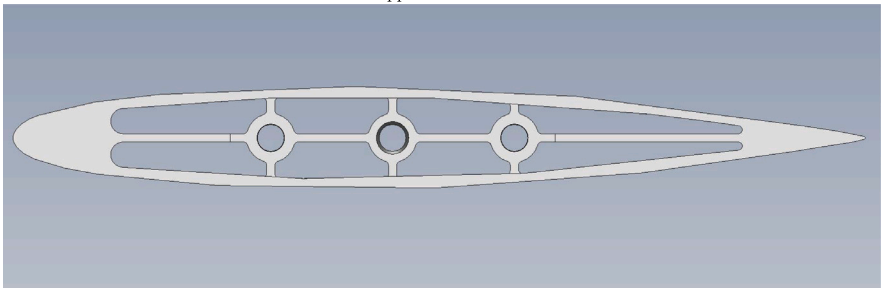

(d) Airfoil configuration

Fig. 3. Control system of actively controlled airfoils.

supporting rods can be separated to replace the outer configurations conveniently according to different requirements.

The airfoil section shape chosen in is NACA 0012-64 (Zhang et al., 2015) with 210 mm chord length, and the other dimensions are scaled up according to the dimensionless coordinates of the NACA 0012-64 airfoil in Fig. 3(d). The length of an airfoil is 1450 mm, the spacing between adjacent airfoils is about 150 mm, and the blocking rate of airfoils is close to 100% while the torsion angle reaches 45°. The relationship between the torsional amplitude and the motion frequency is shown in Table 1. After the installation of airfoils, the internal view of actively-controlled wind tunnel is shown in Fig. 4.

Table 1
Motion limitation of the airfoil system.

Frequency	Angle limitation
$n < 5$ Hz	±40°
5 Hz $\leq n <$ 10 Hz	±15°
10 Hz $\leq n <$ 15 Hz	±10°

3. Iteration-based simulation method for active flow

3.1. Basic mathematical principles

The basic simulation mechanism of the actively controlled wind tunnel is to find out the deterministic function relationship between input voltage signals and measured wind field characteristics:

$$\boldsymbol{y}^{\text{out}} = f(\boldsymbol{x}^{\text{in}}) \tag{1}$$

in which $\boldsymbol{x}^{\text{in}}$ is the input voltage signals controlled by the active equipment such as fans and fins, and it contains the fan speed and the torsion angle of airfoils; $\boldsymbol{y}^{\text{out}}$ represents the simulated wind characteristics at the desired location of wind tunnel. It can be wind spectrum, average wind speed or other wind field parameters researchers are interested in.

Fig. 4. Internal view of the installed airfoils at the downstream of fans.

Generally, the air inside the wind tunnel has the mass inertia and turbulent flow needs to travel certain distance until reaching the measured location, the velocity history of the generated flow deviates inevitably from the input data. Therefore, the input-measurement relationship of the active wind tunnel is quite complex, and it is very difficult to obtain clear and explicit function $f(\cdot)$ through theoretical derivation or other direct methods. In order to obtain the corresponding input signal $\boldsymbol{x}_*^{\text{in}}$ from the final simulation target $\boldsymbol{y}_*^{\text{out}} = f(\boldsymbol{x}_*^{\text{in}})$, an iterative procedure is performed according to the Banach fixed-point theorem (Banach, 1922), and the Eq. (1) can be rewritten in:

$$\frac{\boldsymbol{y}_*^{\text{out}}}{f(\boldsymbol{x}_*^{\text{in}})}\boldsymbol{x}^{\text{in}} = \boldsymbol{x}^{\text{in}} \tag{2}$$

Defining $g(\boldsymbol{x}^{\text{in}}) = \frac{\boldsymbol{y}_*^{\text{out}}}{f(\boldsymbol{x}_*^{\text{in}})}\boldsymbol{x}^{\text{in}}$, $g(\boldsymbol{x}^{\text{in}}) = \boldsymbol{x}^{\text{in}}$ is called a self-mapping. If, fortunately, the iterative process of the active wind tunnel converges (It states conditions sufficient for the existence and uniqueness of the solution of $g(\boldsymbol{x}^{\text{in}}) = \boldsymbol{x}^{\text{in}}$), this theorem will provide us with a constructive procedure for getting better and better approximations of the fixed point along with certain error bounds. Given an initial value $\boldsymbol{x}_0^{\text{in}}$, $\boldsymbol{x}_1^{\text{in}}$ equals to $g(\boldsymbol{x}_0^{\text{in}})$; when the input signal is $\boldsymbol{x}_1^{\text{in}}$, $\boldsymbol{x}_2^{\text{in}}$ is noted as $g(\boldsymbol{x}_1^{\text{in}})$, and so on. In this sense, the solution of Eq. (2) can be expressed as calculating recursively a sequence $\boldsymbol{x}_{n+1}^{\text{in}} = g(\boldsymbol{x}_n^{\text{in}})$. Since $\{\boldsymbol{x}_n^{\text{in}}\} \to \boldsymbol{x}_*^{\text{in}}$, it is clear that the distance between $\boldsymbol{x}_n^{\text{in}}$ and $\boldsymbol{x}_*^{\text{in}}$ could be as small as we need by choosing n sufficiently large.

The process of obtaining the input with target wind characteristics in the active wind tunnel can be abstracted into the form of the above equation. All we need to do is to construct a suitable iterative formula according to the target wind characteristics. For example, in the active wind tunnel, a specific wind speed time history $\boldsymbol{U}_*^{\text{in}}$ can be simulated by the appropriate input fan speed $\boldsymbol{u}_*^{\text{in}}$. Based on the formula $g(\boldsymbol{u}^{\text{in}}) = \frac{\boldsymbol{U}_*^{\text{out}}}{f(\boldsymbol{u}_*^{\text{in}})}\boldsymbol{u}^{\text{in}} = \boldsymbol{u}^{\text{in}}$, the actual observed wind speed $\boldsymbol{U}_n^{\text{out}}$ become closer to the target $\boldsymbol{U}_*^{\text{out}}$ with updating the $\boldsymbol{u}_n^{\text{in}}$ continuously. Although the specific input-measurement relationship of the wind tunnel is not known in advance, the output of each input can still be obtained by directly inputting the signal to the wind tunnel and then actually measuring, which is consistent with the above process. Therefore, a reasonable design of the iteration method can obtain the wind tunnel input corresponding to the target wind characteristics, and it has been confirmed by subsequent experiments that this method is completely feasible.

3.2. The simulation location and scale ratio

Based on the above Banach fixed-point theorem, two types of non-synoptic wind environments, typhoon and mountain wind, have been reconstructed in the active wind tunnel. For 2-D wind spectra of landing typhoon, the model scale of wind tunnel simulation is chosen as: the length scale ratio is 1/3, the wind speed scale ratio is 1/6, and the corresponding frequency scale ratio is 1/2. The simulation range of target wind spectrum in frequency domain is chosen as 0.1–2.5 Hz. The typhoon spectra could be used for wind tunnel tests of small-scale components such as hangers and cables. The simulation position selected in the test section is 1.93 m from the air outlet and 1.18 m from the center of the airfoils, as shown in Fig. 5. The simulated site is chosen to be sufficiently near the airfoils to prevent the vertical flow characteristics from rapidly decreasing with distance.

Three cobra probes, with a sampling frequency of 1000 Hz, are arranged along the vertical line in the cross section of the wind tunnel. The central position (0.9 m from the ground, point B) is the standard point of the simulation, whose data is collected as the iterative basis. A and C are used to monitor the uniformity of the simulated wind field and not involved in the iterative process. The arrangement of probes is plotted in Fig. 6. As for the non-stationary mountain wind, the geometric scale ratio and the wind speed scale ratio are selected as 1/60 and 1/2, respectively. The installation positions of the cobra probes are the same as those of typhoon wind spectra measurement. The section model test of long-span bridges could make use of the reproduced mountain winds.

4. Application Example 1: 2-D wind spectra of landing typhoons

4.1. An introduction to wind spectra of typhoon Hagupit (0814)

The first simulation object is the 2-D wind spectra in typhoon landing, typhoon Hagupit is taken as the example. In Fig. 7, the wind speed data of typhoon Hagupit is divided into 144 sequences and each lasts 10 min. As a large-scale air rotating system, the typhoon wind field structure is affected by plenty of parameters such as the radius to maximum wind speed, the radial pressure profile shape parameter, the local terrain roughness and so on, which makes the turbulence characteristics of the whole typhoon event often time-varying and region-dependent (Fang et al., 2021). Cao et al. (2009) and Xu and Zhan (2001) showed that the wind spectra under typhoon climates are in good agreement with the von Kármán modal at low frequencies. The von Kármán spectra are often defined as:

$$\begin{aligned}\frac{nS_{uu}}{\sigma_u^2} &= \frac{\frac{4L_u n}{U}}{\left[1+70.8\left(\frac{L_u n}{U}\right)^2\right]^{5/6}} \\ \frac{nS_{ww}}{\sigma_w^2} &= \frac{4L_w n}{U}\frac{1+755.2\left(\frac{L_w n}{U}\right)^2}{\left[1+282.8\left(\frac{L_w n}{U}\right)^2\right]^{11/6}}\end{aligned} \tag{3}$$

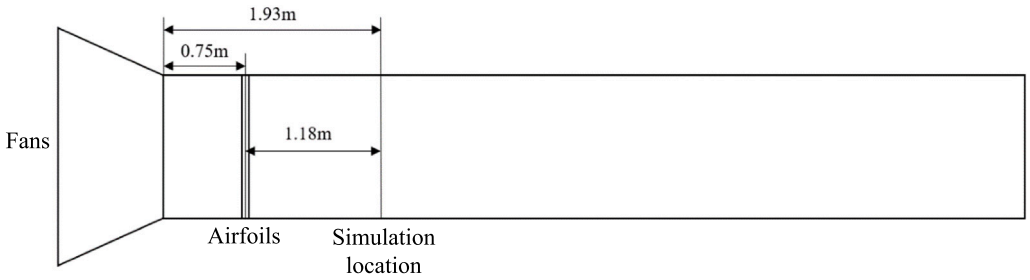

Fig. 5. Simulation location diagram.

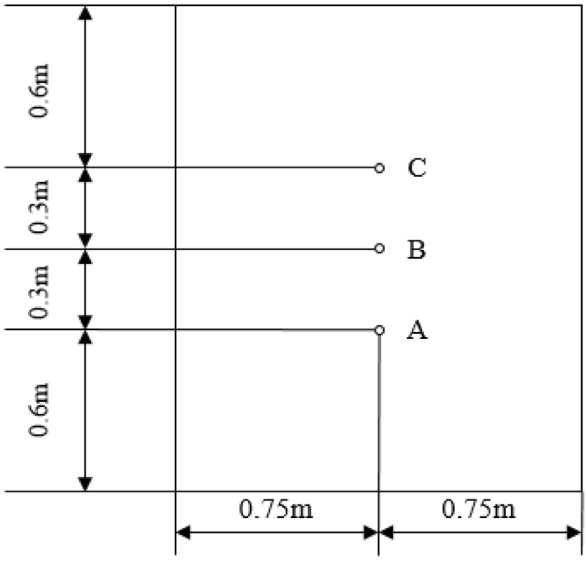

(a) Sketch map

(b) Physical map

Fig. 6. Installation position of cobra probes.

in which, U is the wind speed, n is the Hz frequency, L_u and L_w are the turbulence integral scales in the along-wind and vertical directions, respectively, and σ_u and σ_w are the corresponding turbulence intensities. On the other hand, deviations from the Karman-type spectra have also been noticed in the field measurement of typhoon (Zhao et al., 2019). The energy of high-frequency region in these special typhoon spectra is larger than that in macro-scale synoptic winds (Caracoglia and Jones, 2009).

With the calculation of wind spectra of the whole process of Hagupit, there are a small part of wind spectra that have an upward trend at high frequencies, which make it is inappropriate to use the von Kármán spectrum to fit all the measured data. For this reason, the wind spectra of typhoon Hagupit are divided into two categories in Fig. 8. The first type is the wind spectrum matching the von Kármán spectrum, and the second type is the one deviating from the von Kármán spectrum. The measured spectrum and the fitted spectrum of these two categories are given in Figs. 9 and 10, which are derived from the 46th (Conforming to von Kármán spectrum) and 113th (Deviating from von Kármán spectrum) wind speed time histories. Because there is still no consensus on the general properties of the power spectrum density (PSD) of typhoon (Zhao et al., 2019), for the typhoon wind spectra of non-Kármán types, they are all fitted by the double logarithmic third-order polynomial:

$$\lg(S(n)) = \sum_{i=0}^{3} a_i (\lg(n))^i \tag{4}$$

where $S(n)$ is the longitudinal or vertical PSD and a_i are the fitted parameters. Compared with the von Kármán spectrum with a clear theoretical formula, the non-synoptic spectrum is challenging to be reproduced by modifying wind characteristics like wind speed, turbulence and integral scale. The simulation procedure needs to be realized in the whole frequency domain.

4.2. The method of reproducing 2-D wind spectra

The simulation process of 2-D wind spectrum is based on the characteristics of the experimental devices and the simulation process of 1-D wind spectrum. The energy distribution in the frequency domain is modified in each wind spectrum simulation, and it is then transformed into the time histories of fans and fins which are put straight into the devices' servomotors. The wind tunnel system composed of actively controlled fans and airfoils system is semi-coupled in simulating wind spectrum. In the appropriate wind velocity range, when the input time history of the fans is changed, it only affects the longitudinal PSD. Differently, when the input time history of the airfoils is changed, it not only determines the vertical PSD, but also influences the longitudinal PSD. Therefore, according to an iteration-based method recommended by Cao et al. (2001), the 2-D wind spectra are reproduced in the following procedure (Fig. 11):

Step 1: Firstly, the vertical wind spectrum is simulated by airfoils. The fan speed is fixed to the average wind speed U_{mean}, and the initial input signal PSD $S_{ww}^{0,i}(n)$ of airfoils' servomotors equals to the target vertical turbulence PSD $S_{ww}^{t}(n)$. The corresponding time series of airfoil

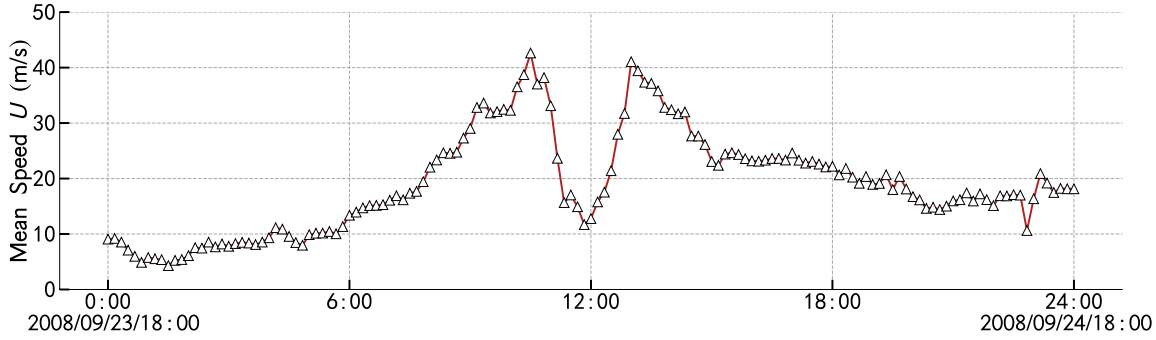

Fig. 7. Average wind speed development during typhoon Hagupit.

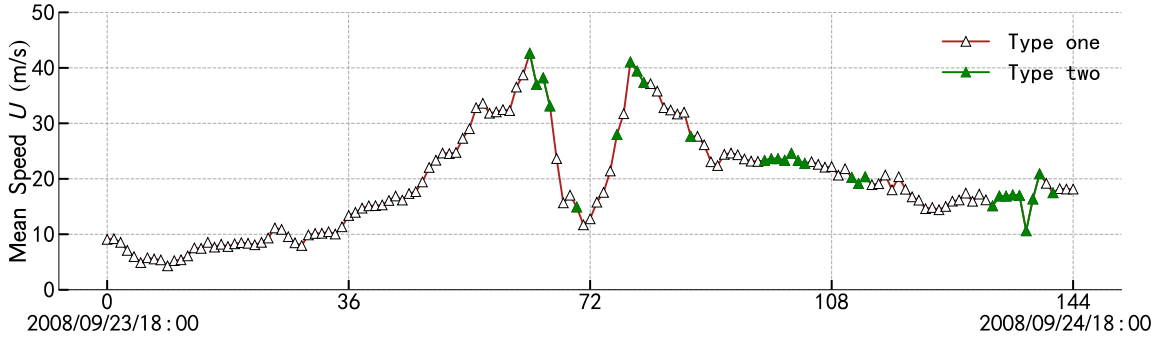

Fig. 8. PSD classification during typhoon Hagupit.

pitching can be generated by Shinozuka's theory (Shinozuka and Jan, 1972). The measured vertical PSD $S_{ww}^{1,m}(n)$ for the first time usually differs from the target wind spectrum $S_{ww}^{t}(n)$. The input data of the airfoils should be modified by the following iteration formula:

$$S_{ww}^{k+1,i}(n) = S_{ww}^{k,i}(n)\frac{S_{ww}^{t}(n)}{S_{ww}^{k,m}(n)} \tag{5}$$

in which $S_{ww}^{k,i}(n)$ is the PSD of airfoil motion for iteration k, and $S_{ww}^{k,m}(n)$ is the measured vertical turbulence PSD for iteration k. Generally, the PSD error e_0 should decrease with the number of iterations increases, and the vertical turbulence is successfully simulated until e_0 is acceptable enough. If the PSD cannot converge to a determined value, the simulation will fail.

Step 2: Make the active airfoils run continuously in line with the input time series obtained in step 1. Based on Eq. (2), the vertical PSD is generated by the iteration formula as follows:

$$S_{uu}^{k+1,i}(n) = S_{uu}^{k,i}(n)\frac{S_{uu}^{t}(n)}{S_{uu}^{k,m}(n)} \tag{6}$$

in which $S_{uu}^{t}(n)$ is target longitudinal turbulence PSD, $S_{uu}^{k,i}(n)$ is the PSD of input signal of fan speed for iteration k, and $S_{uu}^{k,m}(n)$ is the measured longitudinal turbulence PSD for iteration k. Also, the longitudinal turbulence is successfully simulated only when the PSD error is small enough.

Step 3: The target 2-D power spectra involving the vertical and horizontal PSD can be reproduced by running the obtained time series of fans and airfoils at the same time.

4.3. Generating 2-D wind spectra

For simplicity and generality, the 63rd time sequence is simulated in the wind tunnel test, whose mean velocity U_{mean} = 6.96 m/s. The fluctuating speeds and spectra after scaling are shown in Figs. 12 and 13. It can be found that the double logarithmic third-order polynomial can well fit the wind spectra accurately. As shown in Fig. 14(b), the vertical power spectrum is first simulated. Obviously, in the first iteration, there is a significant deviation between the vertical wind spectrum and the target wind spectrum. After four runs, the error reaches an acceptable range. Then, the longitudinal turbulent flow is simulated with the grids' motion unchanged. The reproduction of longitudinal turbulence has undergone three runs in Fig. 14(a). The final results are obtained by directly superimposing the vertical wind spectrum and the longitudinal wind spectrum.

5. Application Example 2: 2-D non-stationary wind speed of mountain wind system

5.1. An introduction to the wind climate of mountain areas around Murong Bridge

In mountainous areas, the synoptic system cannot control local fluid field completely because the deep valley area provides time-dependent temperature gradients, so the wind speed and wind direction of the Y-shaped canyon are dominated by local terrain and large-scale monsoon synchronously (Yang et al., 2022). Different from a conventional plain area, the non-stationary inflow has been measured in the mountainous area (Li et al., 2021). By adjusting the input sequence of the fans and the airfoils, the active wind tunnel provides the potential of simulating the non-stationary characteristics of the mountain wind, namely, the time-varying mean wind speed and the angle of attack (AOA).

The wind velocity data used in this paper comes from the field measurement on Murong Bridge in southwestern China. The bridge site is located on the Xianshui River in Yajiang County, Ganzi Prefecture, Sichuan Province. The terrain around the bridge site is shown in Fig. 15, which is a typical narrowed deep-cut canyon with the depth of about 500–1500 m. The valley bottom elevation is about 2600 m and the bridge deck elevation is about 2800 m. Due to the influence of altitude and regional geomorphology, the wind speed at the bridge site is high and sudden wind with great change of wind speed in a short time is easy to happen. The measuring devices including one 3 Axis Ultrasonic anemometer (WindMaster, 32 Hz sampling rate,

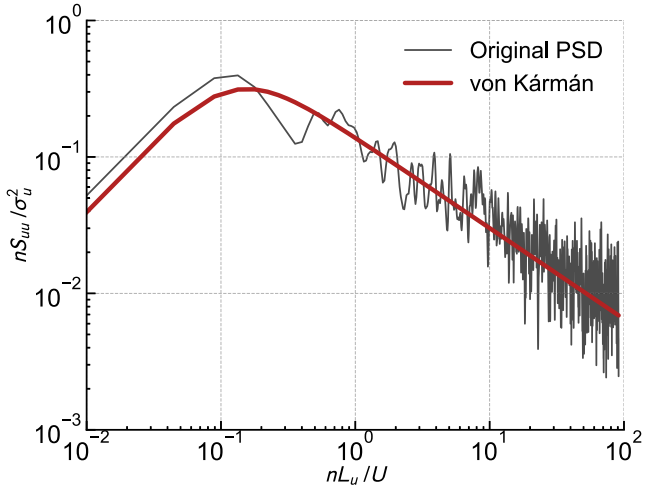

(a) Longitudinal turbulence (U = 16.60 m/s, L_u = 302.8 m, I_u = 0.098)

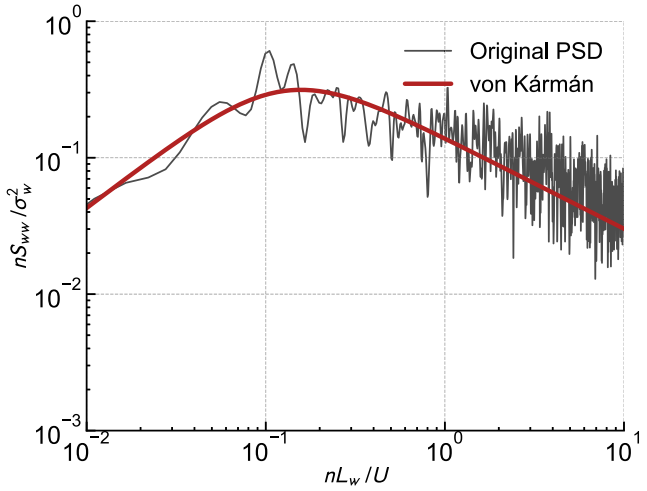

(b) Vertical turbulence (U = 16.60 m/s, L_w = 37.6 m, I_w = 0.045)

Fig. 9. Typhoon wind spectra matching to von Kármán spectrum (sequency No. 46).

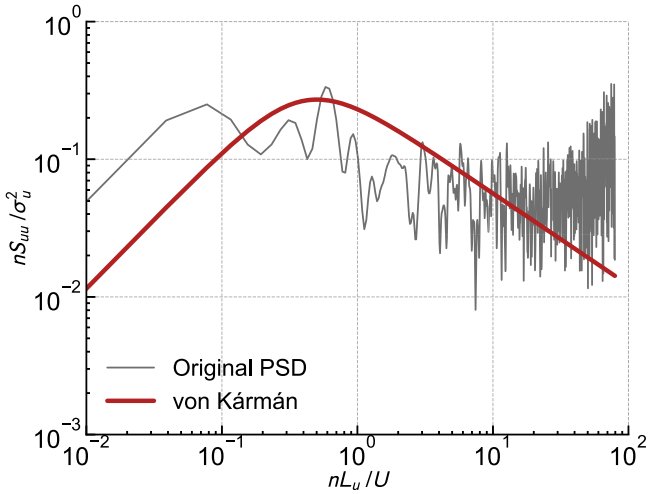

(a) Longitudinal turbulence (U = 19.05 m/s, L_u = 302.5 m, I_u = 0.110)

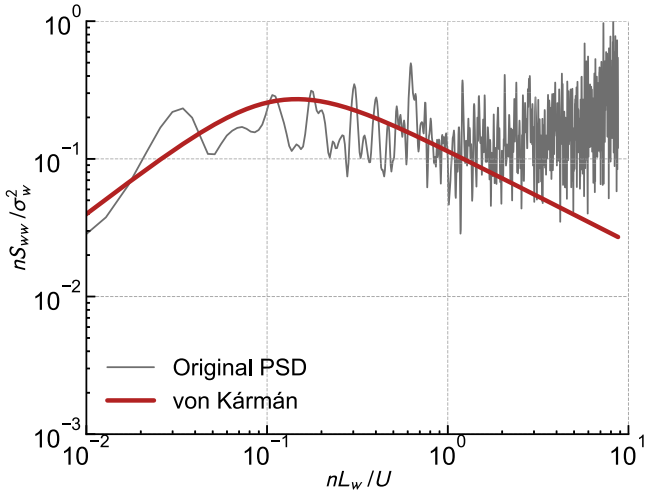

(b) Vertical turbulence (U = 19.05 m/s, L_w = 33.4 m, I_w = 0.050)

Fig. 10. Typhoon wind spectra deviating from von Kármán spectrum (sequency No. 113).

measurement range 0–50 m/s) and one propeller anemometer (RM Young 05103, measurement range 0–60 m/s) were installed on the top of the tower crane, which collected and uploaded wind speed data continuously from December 2019 to September 2020. More details about this field measurement can be seen in Ma et al. (2022).

5.2. The method of reproducing non-stationary wind

The time-varying characteristic of the mean speed is generated by controlling the rotational speeds of the fans, while the AOA is mainly achieved by adjusting the pitching angles of the airfoils. Wind speed is a time-domain parameter that can be directly treated as an input value to the servomotors, without the demand for the conversion from frequency to time domain like PSD simulation. However, reproducing the wind speed and AOA is a mutually coupled process, which means that regardless of the motion of fins or fans will affect the wind speed in two directions simultaneously. The 2-D non-stationary wind simulation cannot be decomposed into the direct superposition of two simulation results of velocity components. Therefore, the iteration process (Fig. 16) of the 2-D non-stationary wind is recommended as follows:

Step 1: Taking the longitudinal wind speed as the first simulation object. The initial input value $U^{0,i}(t)$ for the fan array is chosen as the target time-varying velocity $U^t(t)$. The following correction formula is then introduced:

$$U^{k+1,i}(t) = U^{k,i}(t)\frac{U^t(t)}{U^{k,m}(t)} \tag{7}$$

where $U^{k,i}(t)$ is the time series of input signal for fans' servomotors for iteration k and $U^{k,m}(t)$ is the measured time-varying mean wind speed for iteration k. The ratio of the measured wind speed $U^{k,m}(t)$ to the target wind speed $U^t(t)$ at each time t is regarded as the correction factor for the input wind speed $U^{k,i}(t)$. As the iteration formula converges, this factor tends to approach 1.

Step 2: The AOA of the active airfoils is continuously adjusted to generate the corresponding time-varying wind AOA. The fan array operates according to the final iteration result obtained in Step 1. Similarly, the pitching angle of airfoils is modified by:

$$\alpha^{k+1,i}(t) = \alpha^{k,i}(t)\frac{\alpha^t(t)}{\alpha^{k,m}(t)} \tag{8}$$

where $\alpha^{k,i}(t)$ is the time series of input voltage signal for airfoils' servomotors for iteration k, and $\alpha^{k,m}(t)$ is the measured AOA for iteration k.

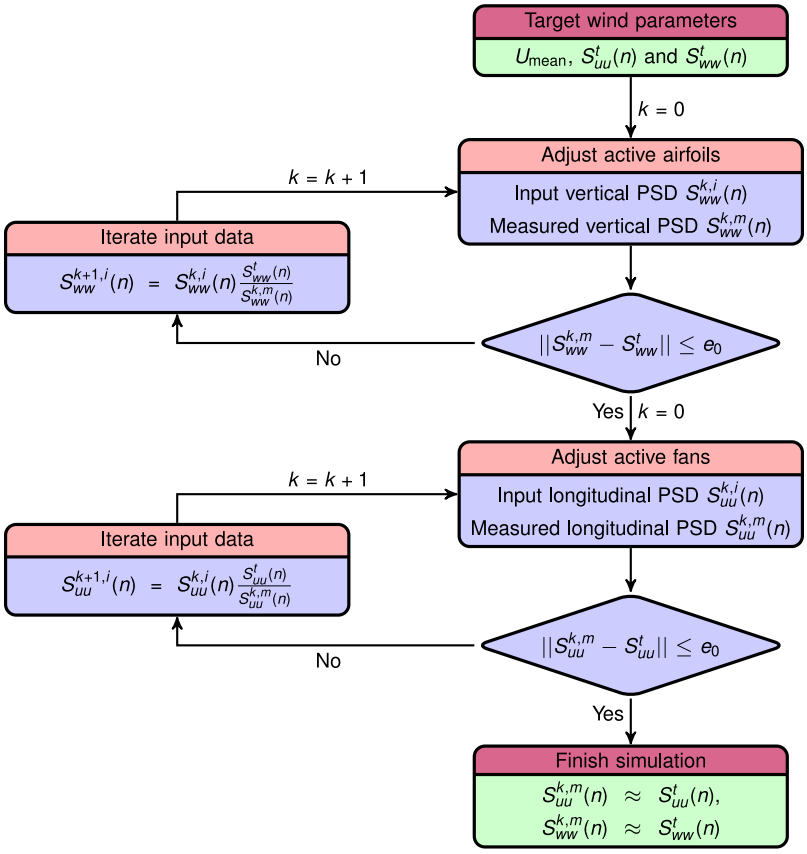

Fig. 11. Flowchart for the reproduction of 2-D wind spectrum.

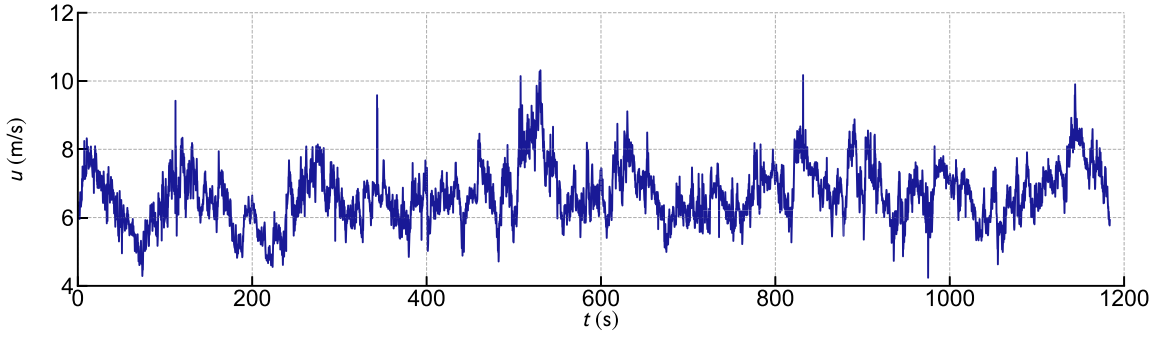

(a) Longitudinal turbulence

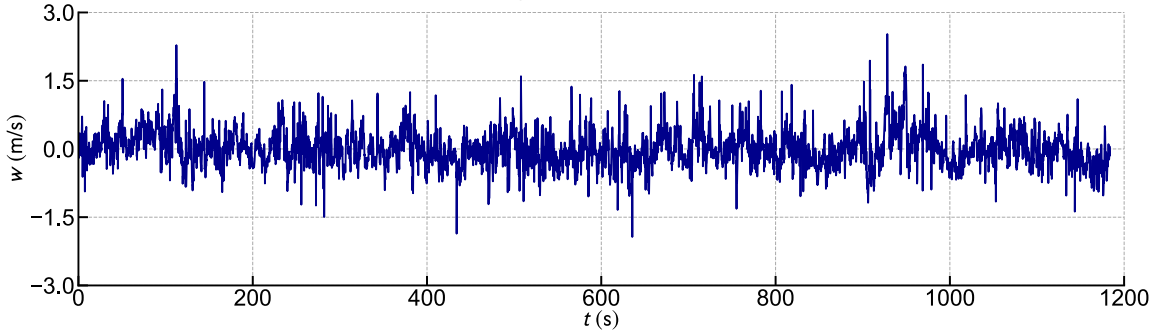

(b) Vertical turbulence

Fig. 12. Scaled fluctuating wind time history.

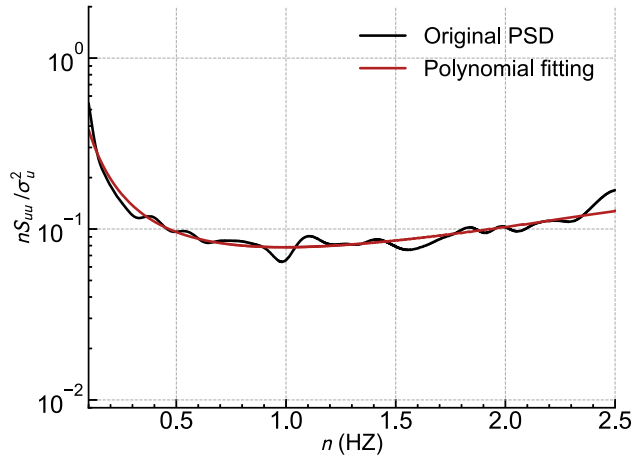

(a) Longitudinal turbulence ($a_0 = -1.54, a_1 = -1.01, a_2 = -1.07, a_3 = 0.42$)

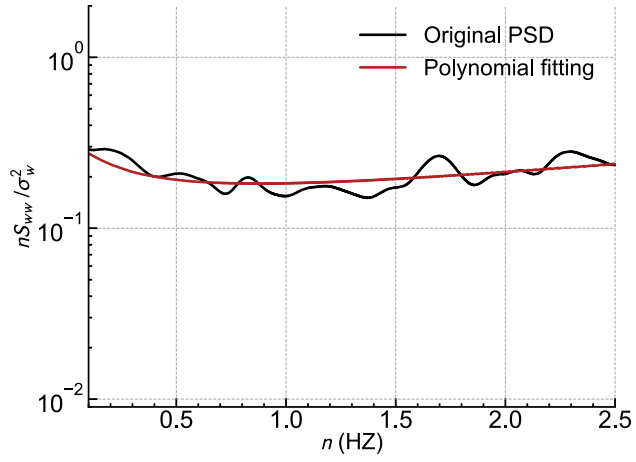

(b) Vertical turbulence ($a_0 = -1.64, a_1 = -0.94, a_2 = -0.46, a_3 = 0.23$)

Fig. 13. Scaled wind spectra.

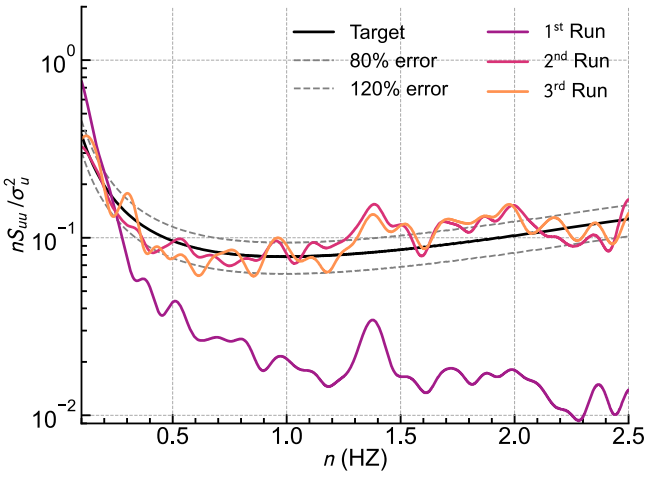

(a) Longitudinal turbulence

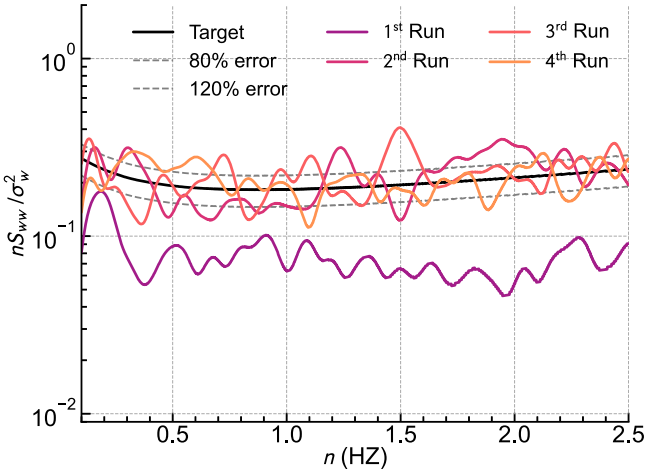

(b) Vertical turbulence

Fig. 14. Iteration process of generating typhoon wind spectra.

After iterations, if the AOA converges to the target value, it means the angle simulation has succeeded.

Step 3: As adjusting the airfoil motion affects the characteristics of the longitudinal flow, it should be checked whether the time-varying mean wind speed still satisfy the error requirements after the modification of AOA. If the error keeps small enough, the simulation of 2-D non-stationary wind field will be complete. Otherwise, use the obtained input data of airfoils and fans as updated initial values and repeat Step 1 and Step 2 until the final result meets the requirement. It should be noted that the iteration of mountain wind is typically less prone to convergence and more time-consuming compared with the 2-D typhoon spectra because extra iteration rounds have to be introduced to make the wind speed and the AOA closer to target values at the same time.

5.3. Generating 2-D non-stationary wind

The wind speed and the AOA after scaling are shown in Fig. 17. Considering the limitation of the frequency and the amplitude of airfoils' torsion, the rapidly changing and large AOA is usually difficult to converge, so the time history of angle is fitted by parabola and reduced to 1/8 of the measured results. To achieve a larger AOA, it may be necessary to improve the shape and arrangement of airfoils or enhance the motion performance provided by AC servomotors.

Firstly, the fan speed is adjusted constantly to approach the target wind speed under the condition that the grids are stationary. As shown in Fig. 18(a), there are four runs until the error meets the requirements. Then, the pitching angle of the airfoils is transformed to simulate the vertical wind speed. The iterative process of the vertical wind speed is given in Fig. 18(b). At this time, as shown in Fig. 19, the movement of the airfoils influences the longitudinal wind speed and causes the average velocity to deviate from the target value, which means that a new iteration of longitudinal speed needs to be started.

In Fig. 20, the wind speed and AOA are iterated again. Since the input voltage of the grids depends on the result of the first iteration, the interference of adjusting the wind AOA on the longitudinal direction should be less than before. As shown in Fig. 21, the average wind speed and AOA can meet the requirements at the same time after the second iteration.

6. Conclusions

This study proposes to simulate the 2-D flow characteristics of the unconventional wind environments in the updated active wind tunnel. A mechanical system has been designed to update the original actively controlled wind tunnel, and airfoils with the shape of NACA 0012-64 are installed to improve the simulation accuracy of vertical flow. Due to the fact that the direct generation of 2-D wind field in the active tunnel is quite complicated, an iterative method is applied to adjust the input signal of the servomotors to approach the target wind

Fig. 15. Terrain at the bridge site (Captured from Google Earth) (Ma et al., 2022).

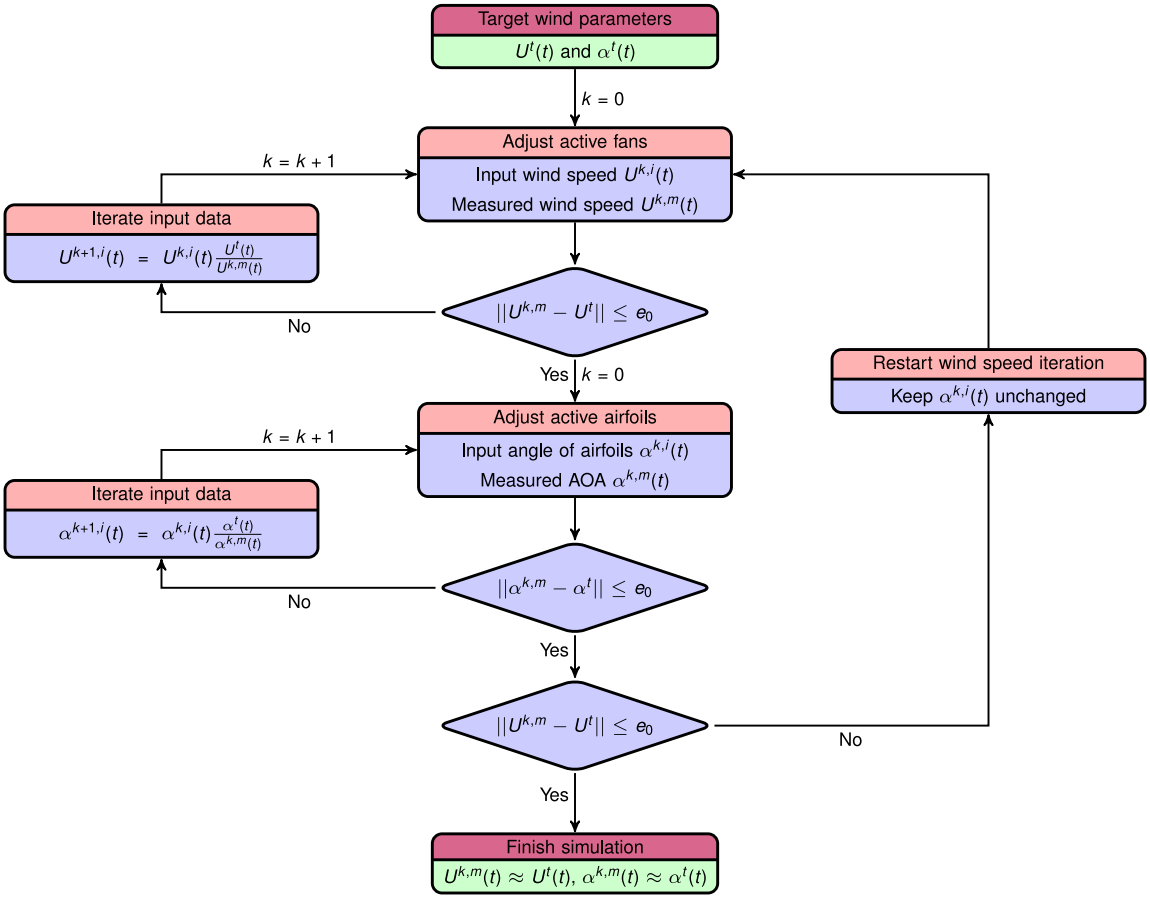

Fig. 16. Flowchart for the reproduction of 2-D non-stationary wind.

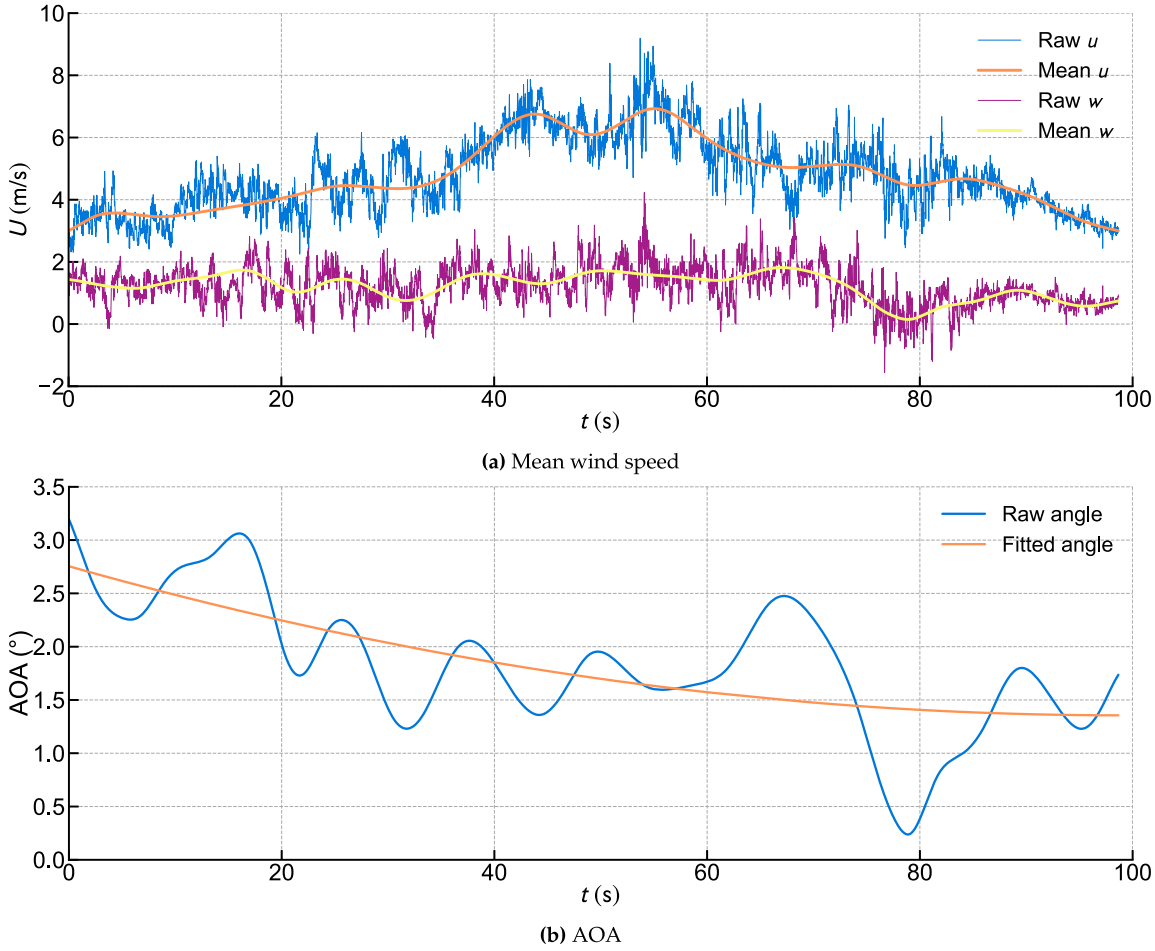

(a) Mean wind speed

(b) AOA

Fig. 17. Time series of the simulated mountain wind.

parameters. Then, two typical non-synoptic wind climates, the typhoon wind spectra and the non-stationary wind speeds of the mountain wind system, were reproduced successfully. The specific iteration processes are developed based on the dissimilar generation features of wind spectra (semi-coupling) and speeds (full-coupling). The longitudinal spectrum and the vertical spectrum are relatively independent in the simulation process, which makes the reproduction of the 2-D wind spectrum can be decomposed into that of two 1-D wind spectra. Differently, the non-stationary wind speed and AOA are both controlled by fans and airfoils, so the simulation process must be carried out synchronously for the wind speed and AOA, which greatly increases the simulation duration and the convergence challenge.

In fact, the iterative principle in this work is a broadly applicable technique. If more measurement points are chosen along the height direction and a suitable iterative approach is developed, then theoretically an active wind tunnel will have the potential for producing a 2-D wind parameter profile. The simulation results can be used in the wind-resistant design of high-rise structures such as cooling towers or skyscrapers. Nevertheless, the experimental experience shows that the performance of the active fins has a great influence on the vertical flow. The distance between airfoils and measurement points must be small enough to guarantee the control ability of airfoils over the vertical velocity component of the flow field. In addition, the finished simulation has been limited to small AOA and slowly changing AOA because simulating the large or fast changing AOA often leads to the divergence of the iterative formula and exceeds the regulation range of the test equipment. For further development of the performance of active wind tunnel about the simulation of non-synoptic wind climates, the mechanism of the airfoils on the flow field needs deep investigation and understanding.

CRediT authorship contribution statement

Lin Zhao: Supervision, Funding acquisition. **Liutian Zhang:** Writing – review & editing, Writing – original draft. **Wei Cui:** Supervision, Methodology, Investigation, Funding acquisition. **Shuyang Cao:** Methodology. **Yaojun Ge:** Supervision.

Declaration of competing interest

The authors declare that they have no known competing financial interests or personal relationships that could have appeared to influence the work reported in this paper.

Data availability

Data will be made available on request.

Acknowledgments

The authors gratefully acknowledge the support of the National Key Research and Development Program of China (2022YFC3005302, 2021YFF0502200). Any opinions, findings, conclusions, or recommendations are those of the authors and do not necessarily reflect the views of the agencies mentioned above.

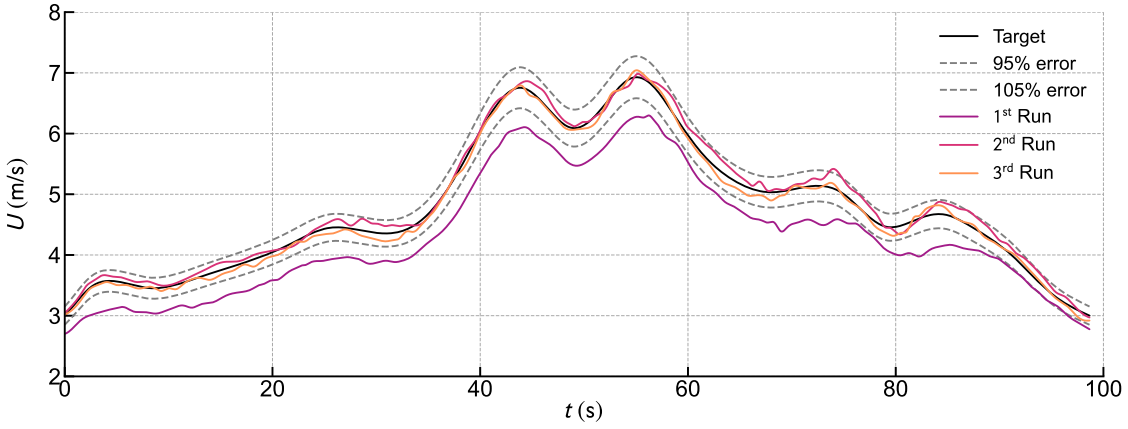

(a) Mean wind speed

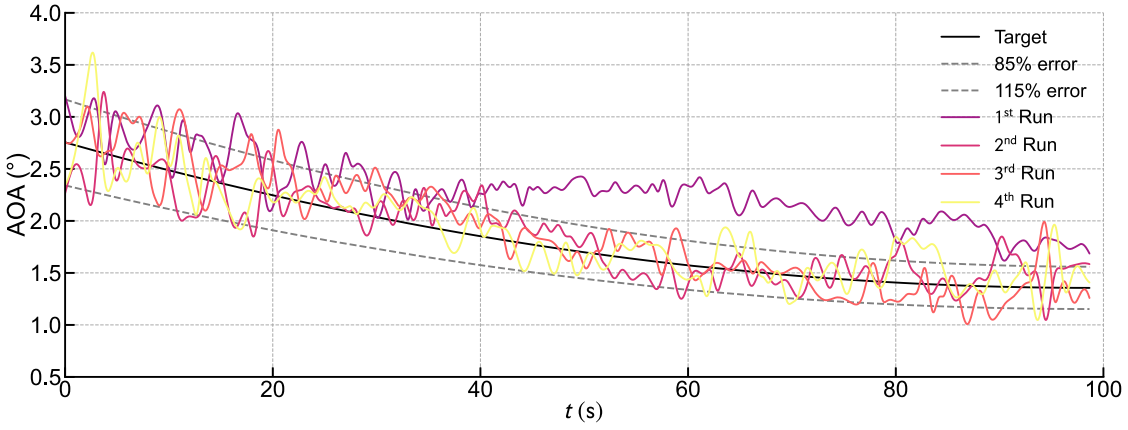

(b) AOA

Fig. 18. The 1st iteration of simulated flow field.

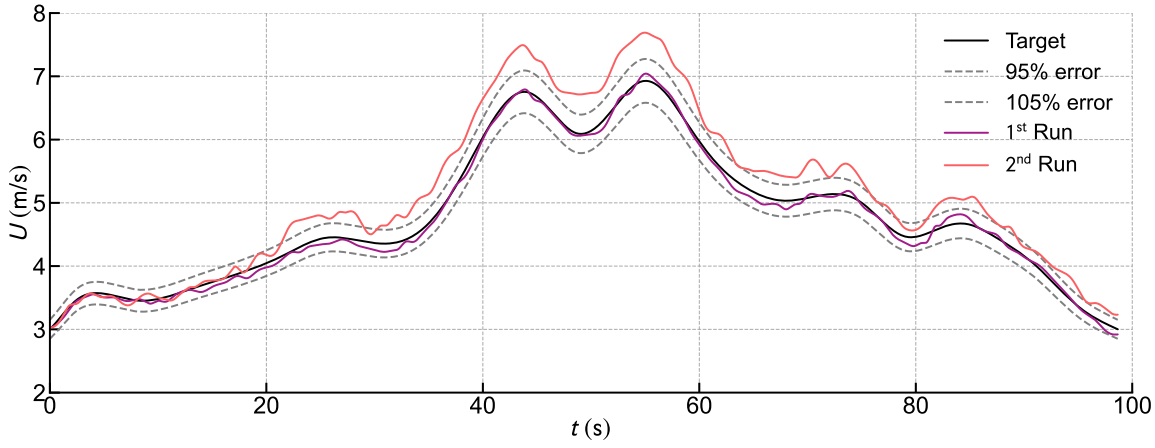

Fig. 19. Longitudinal velocity after the 1st iteration.

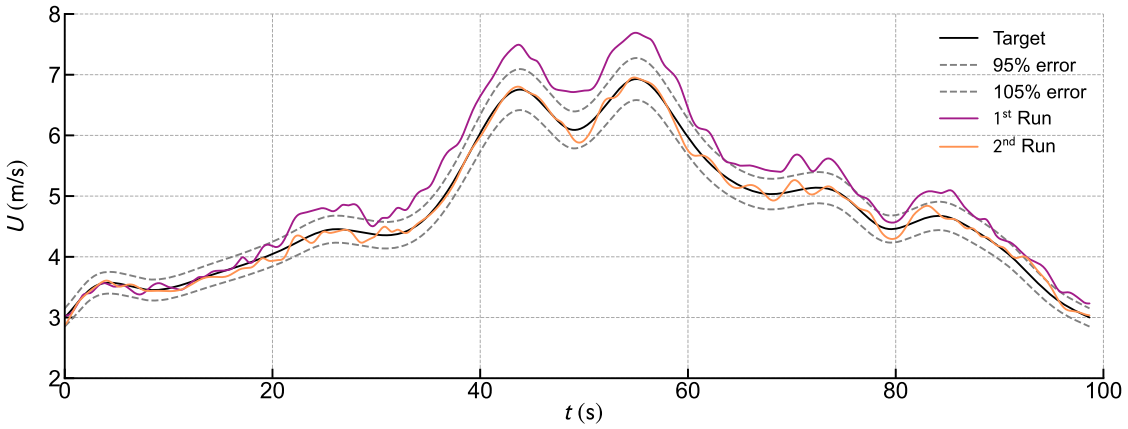

(a) Mean wind speed

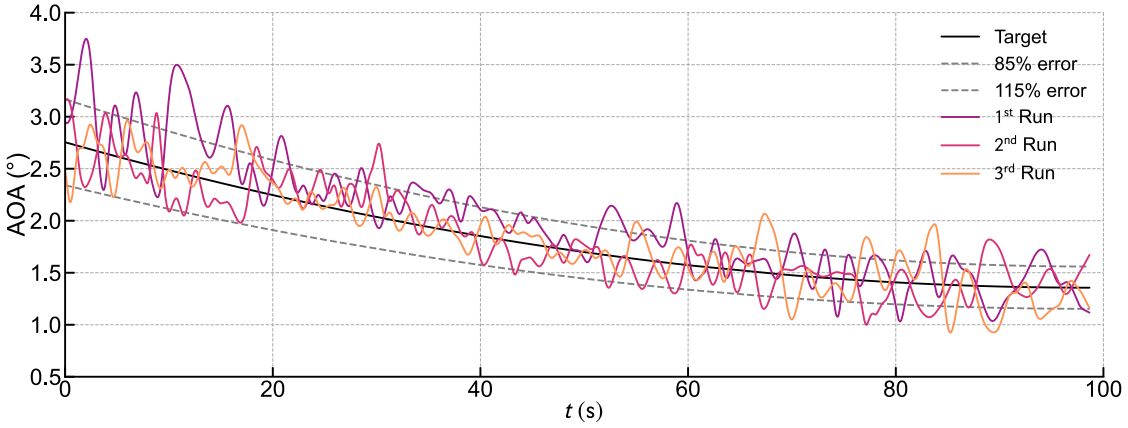

(b) AOA

Fig. 20. The 2nd iteration of simulated flow field.

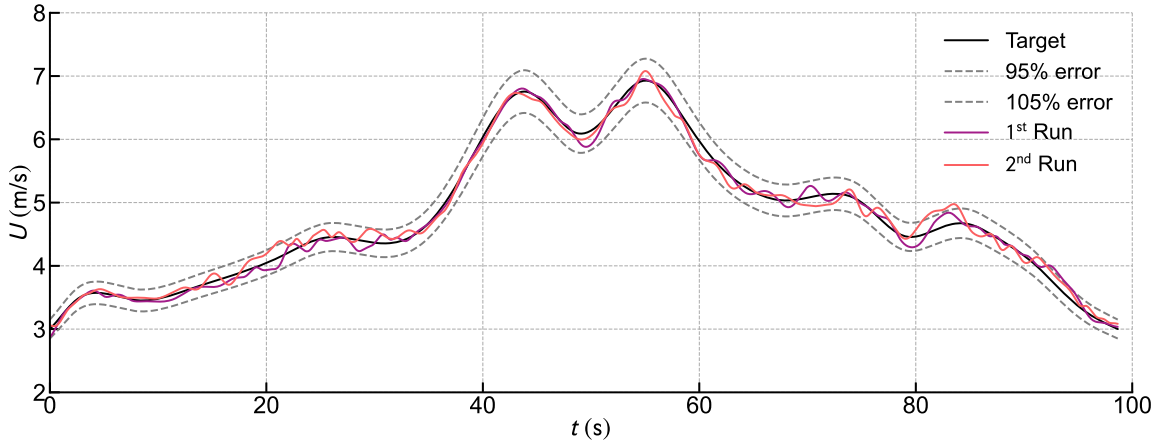

Fig. 21. Longitudinal velocity after the 2nd iteration.

References

Banach, S., 1922. Sur les opérations dans les ensembles abstraits et leur application aux équations intégrales. Fundam. Math. 3 (1), 133–181.

Cao, S., Nishi, A., Hirano, K., Ozono, S., Miyagi, H., Kikugawa, H., Matsuda, Y., Wakasugi, Y., 2001. An actively controlled wind tunnel and its application to the reproduction of the atmospheric boundary layer. Bound.-Layer Meteorol. 101, 61–76.

Cao, S., Nishi, A., Kikugawa, H., Matsuda, Y., 2002. Reproduction of wind velocity history in a multiple fan wind tunnel. J. Wind Eng. Ind. Aerodyn. 90 (12–15), 1719–1729.

Cao, S., Tamura, Y., Kikuchi, N., Saito, M., Nakayama, I., Matsuzaki, Y., 2009. Wind characteristics of a strong typhoon. J. Wind Eng. Ind. Aerodyn. 97 (1), 11–21.

Caracoglia, L., Jones, N.P., 2009. Analysis of full-scale wind and pressure measurements on a low-rise building. J. Wind Eng. Ind. Aerodyn. 97 (5–6), 157–173.

Cermak, J.E., 1995. Progress in physical modeling for wind engineering. J. Wind Eng. Ind. Aerodyn. 54, 439–455.

Cermak, J., Cochran, L., 1992. Physical modelling of the atmospheric surface layer. J. Wind Eng. Ind. Aerodyn. 42 (1–3), 935–946.

Counihan, J., 1969. An improved method of simulating an atmospheric boundary layer in a wind tunnel. Atmos. Environ. (1967) 3 (2), 197–214.

Counihan, J., 1973. Simulation of an adiabatic urban boundary layer in a wind tunnel. Atmos. Environ. (1967) 7 (7), 673–689.
Cui, W., Zhao, L., Cao, S., Ge, Y., 2021. Generating unconventional wind flow in an actively controlled multi-fan wind tunnel. Wind Struct. 33, 115–122.
Cui, W., Zhao, L., Ge, Y., 2022. Non-Gaussian turbulence induced buffeting responses of long-span bridges based on state augmentation method. Eng. Struct. 254.
Dong, X., Zhao, L., Cui, W., Peng, Y., Ge, Y., 2022. Aerodynamics and aeroelastic performance of a rigid-frame bridge with a bluff body girder subjected to short-rise-time gusts. Eng. Struct. 263, 114376.
Fang, G., Pang, W., Zhao, L., Rawal, P., Cao, S., Ge, Y., 2021. Toward a refined estimation of typhoon wind hazards: Parametric modeling and upstream terrain effects. J. Wind Eng. Ind. Aerodyn. 209, 104460.
Fang, G., Zhao, L., Chen, X., Cao, J., Cao, S., Ge, Y., 2020. Normal and typhoon wind loadings on a large cooling tower: A comparative study. J. Fluids Struct. 95, 102938.
Hou, F., Sarkar, P.P., 2020. Aeroelastic model tests to study tall building vibration in boundary-layer and tornado winds. Eng. Struct. 207, 110259.
Irwin, H., 1981. The design of spires for wind simulation. J. Wind Eng. Ind. Aerodyn. 7 (3), 361–366.
Kobayashi, H., Hatanaka, A., 1992. Active generation of wind gust in a two-dimensional wind tunnel. J. Wind Eng. Ind. Aerodyn. 42 (1–3), 959–970.
Kobayashi, H., Hatanaka, A., Ueda, T., 1994. Active simulation of time histories of strong wind gust in a wind tunnel. J. Wind Eng. Ind. Aerodyn. 53 (3), 315–330.
Lei, S., Cui, W., Patruno, L., de Miranda, S., Zhao, L., Ge, Y., 2022. Improved state augmentation method for buffeting analysis of structures subjected to non-stationary wind. Probab. Eng. Mech. 69, 103309.
Li, S., Li, X., Li, J., Su, Y., Wu, B., 2023. Measurements of the unsteady lift force on a 5: 1 rectangular cylinder based on active-passive hybrid wind tunnel tests. Measurement 213, 112674.
Li, Y., Yu, J., Zhang, M., Tang, H., 2021. Wind characteristics of a bridge site and wind-resistance key technology in complex mountains. Sci. Sin. Technol. 51 (05), 530–542.
Liu, Z., Fang, G., Hu, X., Xu, K., Zhao, L., Ge, Y., 2022. Stochastic power spectra models for typhoon and non-typhoon winds: A data-driven algorithm. J. Wind Eng. Ind. Aerodyn. 231, 105214.
Ma, T., Cui, W., Zhao, L., Yejun, D., Genshen, F., Ge, Y., 2022. Extreme wind speed prediction in mountainous area with mixed wind climates. In: Stochastic Environmental Research and Risk Assessment. Springer, pp. 1–19.
Shinozuka, M., Jan, C.-M., 1972. Digital simulation of random processes and its applications. J. Sound Vib. 25 (1), 111–128.
Xu, Y.L., Zhan, S., 2001. Field measurements of di wang tower during typhoon york. J. Wind Eng. Ind. Aerodyn. 89 (1), 73–93.
Yang, W., Liu, Y., Deng, E., Wang, Y., He, X., Lei, M., 2022. Characteristics of wind field at tunnel-bridge area in steep valley: Field measurement and LES study. Measurement 202, 111806.
Zhang, W., Cheng, W., Gao, W., Qamar, A., Samtaney, R., 2015. Geometrical effects on the airfoil flow separation and transition. Comput. & Fluids 116, 60–73.
Zhang, M., Yu, J., Zhang, J., Wu, L., Li, Y., 2019. Study on the wind-field characteristics over a bridge site due to the shielding effects of mountains in a deep gorge via numerical simulation. Adv. Struct. Eng. 22 (14), 3055–3065.
Zhao, L., Cui, W., Ge, Y., 2019. Measurement, modeling and simulation of wind turbulence in typhoon outer region. J. Wind Eng. Ind. Aerodyn. 195.
Zhao, L., Xie, R., Huang, H., Yan, X., Cao, S., Ge, Y., 2023. Aerodynamic characteristics of a streamlined box girder under shear flow considering oncoming turbulence. Phys. Fluids 35 (9).